

Research Article

Mohamed Elhag*

Consideration of Landsat-8 Spectral Band Combination in Typical Mediterranean Forest Classification in Halkidiki, Greece

<https://doi.org/10.1515/geo-2017-0036>

Received Mar 16, 2017; accepted Jul 10, 2017

Abstract: Utilization of satellite data by means of remote sensing practices creates a wider window of opportunities to conduct robust outcomes Landsat OLI-8 data acquired over the peninsula of Halkidiki in Greece for the summer period of 2013, were analyzed to determine their utility to classify natural resources categories based on the determination of spectral bands combination. Consequently, spectral bands combination can be used to classify various categories based on their higher overall accuracy assessment. Spectral information contained in each of the utilized channels of Landsat OLI-8, statistics defining 12 cover type classes of interest were calculated and used as a basis for classification of the designated study area. Spectral bands combinations (4-5-6/ 3-4-5/ 3-4-5-6/ 4-5-6-7) fulfill the required accuracy for forest purpose as they conducted overall accuracies ranging between 7.85% and 96.29%. The spectral band combination 3-4-5-6-7 conducted the highest overall accuracy (98.15%). The poorest results were obtained by the analysis of spectral bands combination 4-6 (68.52%). Single spectral band 6 conducted the best overall results; however, spectral bands 5 and 6 seemed to be the most useful spectral bands combination for each category.

Keywords: Accuracy Assessment, Spectral band Combination, Image Classification, Mediterranean Forest, Remote Sensing Data

1 Introduction

The general term of image processing is to extract information either with no interference with the observed data

(image preprocessing) and/or with adequate interference to improve the results concerning the observed phenomena [1, 2]. The most common practice in image processing is to recognize a pattern. Tou and Gonzalez [3] has defined pattern recognition as the categorization of input data into identifiable classes, via the extraction of significant features or attributes of the data from background irrelevant details [4, 5].

The first step in the analysis sequence involves the selection of data samples from which the computer may drive the necessary statistical parameters for the “training” of the classification algorithm [6, 7]. The training samples are based on “ground truth” information. This means that the used categories are defined based on the separability index [8, 9].

There are two major approaches, the unsupervised and the supervised model. The unsupervised model is useful when the spectral info is not identified [10]. An important criterion for clustering is the minimization of the sum of square error for determining the spectral class composition of the data, prior to detailed analysis by the method of supervised classification [2, 11]. Supervised classification assumes that each spectral class can be described by the probability distribution in the multispectral space; this will be a multivariate distribution with many variables as dimensions of space [12, 13].

Classification costs increase by the number of features which are used to describe pixel vectors in a multispectral space e.g. “with the number of spectral bands associated with a pixel” [14, 15]. Each class has a statistical spread associated with it, through the data point in each spectral band. As such probability distributions, can overlap, to greater or lesser extent; the class separability becomes a function of both the separation of the means and the statistical distribution of data points, within each class, for each dimension [8, 16].

Each of OLI-8 spectral bands can potentially contribute to the multispectral land cover classification. Although, there is a redundancy of information due to high inter-spectral band correlation [17]. Two basic approaches are used to identify subsets of spectral bands, which might

*Corresponding Author: Mohamed Elhag: Department of Hydrology and Water Resources Management, Faculty of Meteorology, Environment & Arid Land Agriculture, King Abdulaziz University Jeddah, 21589. Kingdom of Saudi Arabia; Email: melhag@kau.edu.sa

be suitable classification of the multispectral data. These are separability analysis and evaluation of eigenvector and eigenvalue data derived from class statistics [18, 19]. There are several measures of separability available to predict best spectral bands combination for classification which are based on measurements of the statistical distance between spectral classes of interest [20–22].

According to Gausman *et al.* [23], the wavelength of 0.68, 0.85, 1.65 and 2.20 μm is useful for monitoring vegetation. Lathrop *et al.* [24] reported that the most informative spectral intervals for monitoring for natural materials were 0.54–0.56, 0.66–0.68 and 0.78–0.82 μm . Many researchers are trying to evaluate the best single or combination of spectral bands for displaying, mapping and classifying forest lands [25].

Murtha and Watson [26] stated that a combination of spectral bands, primarily TM 5 and 6 are required for the interpretation and mapping forest clear cuts. Coggeshall and Hoffer [27] verified that at least one spectral band in the near infrared or middle infrared is necessary to accurately discriminate broadleaf and conifers forests. Spanner *et al.* [4] using principal component analysis found that the four optimal spectral bands of the Thematic Mapper Simulator (TMS) data for forest vegetation analysis, over a Northern Idaho study site, were the near infrared (TMS4), thermal infrared (TMS6), mid-infrared (TMS5) and red (TMS3). Latty and Hoffer [1], using average transformed divergence, found the highest separability between South Carolina forest classes in four spectral bands subset consisting of TM 1, –3, –4 and 5. They noted that such waveband selection results were “highly data and application dependent”. Duda *et al.* [28] pointed out that beyond a certain point the inclusion of additional features leads to worse rather than better performance. Nelson *et al.* [1] using stepwise discrimination analysis of TMS data, appeared to provide forest classification accuracies that are not significantly different from similar scholarly work [29, 30].

The main purpose of the study is to increase the knowledge about the use of satellite data in vegetation ecosystems. More specifically the objective is to determine the spectral bands combination that gives the highest overall accuracy that can be used for better classification of various categories of typical Mediterranean land cover.

2 Materials and Methods

2.1 Study Area

The study area is the peninsula Sithonia of the prefecture of Halkidiki (Figure 1). Study area selection was based on the fact that the designated study area belongs to a typical Mediterranean ecosystem. Therefore, most of the major forest cover types found in Greece are presented in the area [31]. Moreover, there are available ancillary data giving information about the vegetation, soil, and topography. Sithonia is situated on the middle of the three peninsulas of Halkidiki and occupies a place with longitude between $23^{\circ} 36'$ up to $24^{\circ} 00'$ E and latitude between $39^{\circ} 56'$ up to $40^{\circ} 14'$ N. The peninsula, with 43 km in length and 6 km in width in the northern part and 18 km in the center, is considered as a continuation of the mountain Holomonta. Its acreage is about 450 km^2 , half of which are covered by forests of Aleppo pine (*Pinus halepensis*), which settles its optimum development in Sithonia. The elevation is up to 823 m (hill Polielaos). The relief is gently looping, but there are places with an inclination of 50–60%. The peninsula has only small numerous water streams with seasonal activity, which create gully erosion phenomena. The pressure of the biotic factors of the area has affected the soil of Sithonia. The main rocks found are granites, metamorphic rocks of gneiss, sandstones, and alluvial rocks, semi-metamorphic rocks of phyllites and calc-schists and finally deposits of alluvial and sand-alluvial rocks [31, 32]. On the east side of Sithonia, where silicate rocks predominate, and the soils are acidic, shallow, with numerous rocks and littler fertility. On these soils, the stand of Aleppo pine of Stone pine (*Pinus pinea*) and Black pine (*Pinus nigra*) have been developed [33]. The understory is composed of acid-friendly bushes of Ericaceae (tree-heath and strawberry tree) and Cistaceae family. On non-silica soils, the maquis has been developed. Moreover, the development of Aleppo pine on such soils is quite better in contrast to the Stone pine [2, 34].

2.2 Data Acquisition

Landsat OLI-8 image was acquired on the 30th of April 2013. It has a nominal center path of 183 and row of 32 according to the Worldwide Reference System. During the processing of the image, Landsat OLI-8 band 1 and the thermal spectral bands were excluded. Spectral band 1 has been omitted because it is highly correlated with spectral band 2, and it's affected by the atmospheric haze [16, 35].

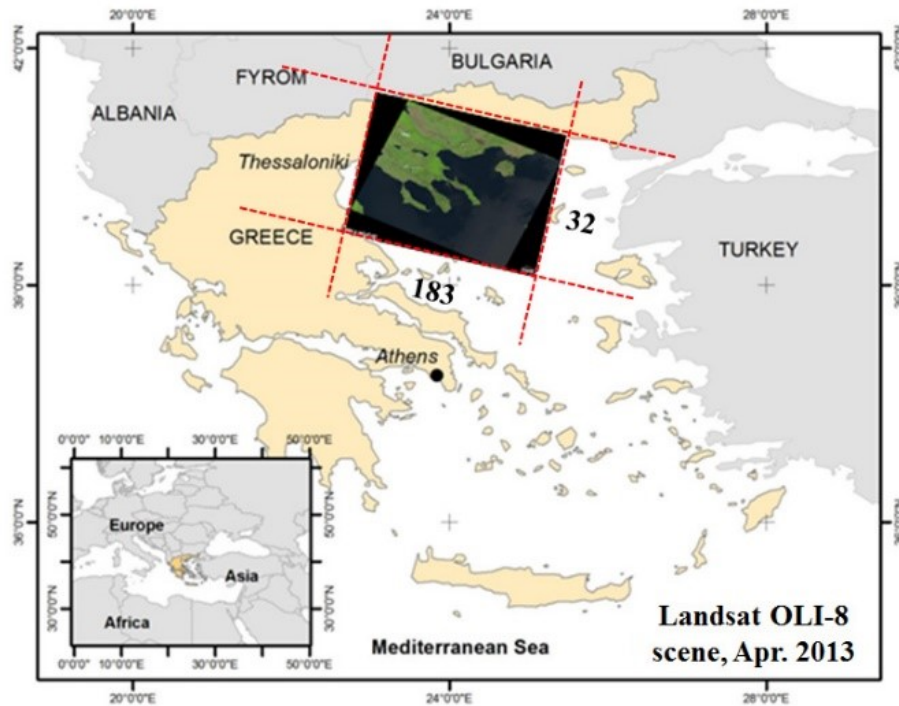


Figure 1: Location of the study area

Thermal spectral bands were excluded from further analysis because they give poor classification results due to their coarse spatial resolution and lack contrast [3, 36, 37]. Ancillary data in the form of thematic maps, orthophotographs, orthophoto maps and aerial photographs were obtained by the Hellenic Army Geographical Service, The Ministry for the Environment, Physical Planning and Public Works and from the Hellenic Forest Service. The vegetation and geological thematic maps (scale 1:500,000) used in this study have been developed by the Directorate of Forest Resources Development, Hellenic Forest Service and by the Institute of Geology and Mineral Exploration.

Field observations have been done during the spring of 2013. The most serious part of the field observations was the accurate recognition of the training sites in the field, in the analog photographs and afterward in the digital images.

2.3 Development of the classification scheme

The classification system proposed by Bonazountas *et al.* [38] has been used for this study. It has been properly adjusted to the Coordination of Information on the Environment “CORINE” Land Cover System (2006). The following classification system was required to establish a list of

12 categories suitable for the study as it illustrated in Figure 2.

2.4 Compilation of classification procedures

2.4.1 Unsupervised classification

An unsupervised classification is an analytical procedure based upon clustering, using different algorithms. The whole image of the study area has been segmented into 12 spectral categories. Various techniques have been used to get more detailed information. In this study we applied the Optimum Index Factor (OIF). The algorithm used to compute OIF for any subset of spectral bands is following Chavez *et al.* [39]:

$$OIF = \frac{\sum_{k=1}^n s_k}{\sum_{j=1}^n Abs(r_j)} \quad (1)$$

Where:

s_k = is the standard deviation from spectral band k .

r_j = is the absolute value of the correlation coefficient between any of the two spectral bands being evaluated.

The spectral bands combination with the largest OIF has the most information, as measured by variance, with the least amount of duplication, as measured by correlation [40, 41].

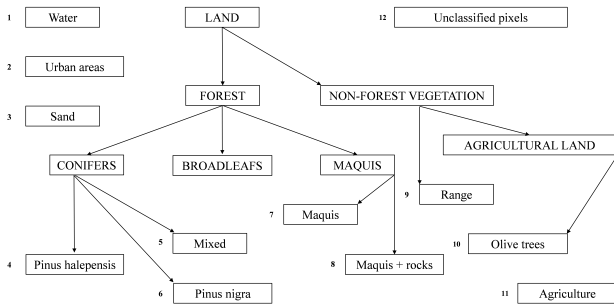


Figure 2: The classification scheme

2.4.2 Supervised classification

A supervised classification is described by the potential distribution of each class in the multispectral dimension. Therefore, it's will be a multivariable distribution with as many variables as the dimensions of the data [42]. A multi-dimensional normal distribution is described as a function of vector location in multispectral space by the following algorithm of Richards and Richards [12]:

$$p(x) = \frac{1}{(2\pi)^{\frac{N}{2}} * |\sum|^{\frac{1}{2}}} * \exp\left(\frac{-1}{2(x-m)}\right)^t * \sum_{-1}^1 (x-y) \quad (2)$$

Where:

x = is a vector location in N-dimensional pixel space.

m = is the mean position of the spectral class.

\sum = is the covariance matrix of the distribution, which describes its spread directionally in the pixel space.

If m and \sum are known for every spectral class in the image, every pixel can be examined and categorized in the most likely class, based on the probabilities computed for the location. In this study, the maximum likelihood classifier has been used, because of its higher accuracy [43, 44].

To do this, an assumption is made that the cloud points forming the category training data is normally distributed [45, 46]. The position of the pixel points in a multispectral space can be described by vectors, whose components are the individual spectral responses in each spectral band. The mean position of the pixels in space is defined by the expected value of the pixel vector "x" according to Richards and Richards [12]:

$$m = E(x) = \frac{1}{k} * \sum_{j=1}^k x_j \quad (3)$$

Where:

m = mean pixel vector.

X_j = individual pixel vectors of total number K.

E = expectation operator.

It is of value to have available a means by which the mean vector defines the average position of the pixels in

multispectral vector space. This is the role of the covariance matrix which is defined as:

$$\sum_x = \frac{1}{k-1} \sum_{j=1}^k (x_j - m) * (x_j - m)^t \quad (4)$$

Where:

t = denote vector transpose.

The covariance matrix is one of the most important mathematical concepts in the analysis of multispectral remote sensing data [47]. So, if there is a correlation between the responses in a pair of spectral bands, the corresponding off-diagonal element in the covariance matrix will be large by comparison to the diagonal terms. On the other hand, if there is a little correlation, the off-diagonal terms will be close to zero [48].

2.5 Accuracy assessment

The final step in the digital image analysis is the evaluation of the accuracy of the classification results. These results are expressed in tabular form are known as a confusion matrix. The statistical analysis presents the accuracy and the misfire of the classification based on the ground truth observations. A distinction is made between errors of omission and errors of commission. Errors of omission corresponded to those pixels belonging to the class of interest that the classifier has failed to recognize, whereas errors of commission are those that corresponded to pixels from other classes that the classifier has labeled as belonging to the class of interest [49]. The omission refers to columns of the confusion matrix, whereas the commission refers to rows.

The following diagram simplifies the methodological framework adopted in the current research study as it's illustrated in Figure 3.

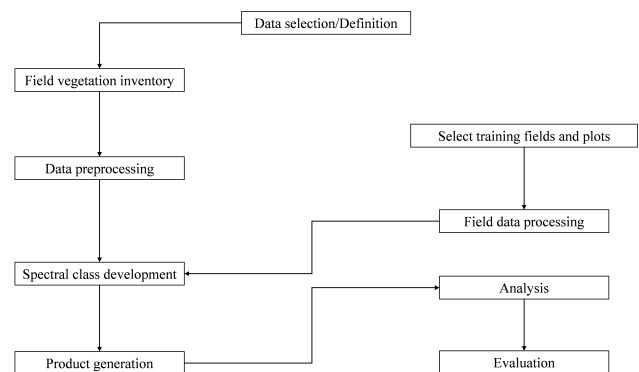


Figure 3: Schematic description of the followed procedures

3 Results and discussion

Unsupervised and supervised procedures based on the spectral bands combinations have been used for the classification of twelve categories in Sithonia peninsula. The unsupervised classification showed low overall accuracy while the supervised showed acceptable overall accuracy for forest purposes. Spectral bands combinations were used for the best discrimination amongst the individual categories.

Once the training fields had been identified, there were grouped according to cover classes. The cover class groups of training fields were then individually clustered to resolve the cover classes into a set of spectral classes. The identified percentages of the quotient classified classes were demonstrated in Figure 4.

The unsupervised classification based on the Iterative Self-Organizing Data Analysis Technique (ISODATA) algorithm was performed using different spectral bands combinations. Table 1 shows the analysis of the classification results based on OIF that were produced. The evaluation of different spectral bands combinations is shown in Figures 5, 6, 7 and 8. In Figure 9, the best spectral bands combinations, based on OIF for the designated study area was reported. Maximum likelihood supervised classification was performed using the best spectral bands combinations based on OIF is shown in Figure 10.

The overall accuracy and the one for each individual category were calculated for each set of analyzed data. This was achieved by using test fields in the study area and random sampling procedure. In this phase, 270 test sites were visited and the data were entered in confusion matrices. This type of representation enables to estimate the omission and commission errors and the overall accuracy of each category of the study area. The results of the overall accuracy are shown in Figure 11.

The overall accuracy assessments ranged from 68.52% to 98.15% and were considered reasonable for forestry purposes by Congalton [49] and Congalton and Green [10]. When spectral bands combination 3-5 (Table 1) was used, the overall accuracy was the lowest (68.52%). The category of conifers was classified with an accuracy ranging from 62.86% (*Pinus nigra*) to 84.44% (*Pinus halepensis*). Also, there were misclassification errors between the categories of *Pinus halepensis* and *Pinus nigra* and mixed conifers, maquis and maquis + rocks, range and agriculture, sand and urban areas, range and maquis according to the statistical separability index. This combination gave the lowest producer's accuracy for the categories of *Pinus nigra*, maquis + rocks and range (62.86, 46.67 and 54.84 re-

spectively) amongst various spectral bands combinations. Most of the forest categories were classified with user's accuracy of less than 80% as the category of maquis showed the lowest accuracy (46.67%).

The spectral bands combination 3-7 (Table 2) gave an overall accuracy of 71.11%. Only a little lower than the spectral bands combinations 3-4-5-6 (71.85%). In this combination, the categories of *Pinus halepensis* and maquis, *Pinus nigra* and mixed conifers, olive trees, and agriculture gave the highest misclassification errors with the lowest producer's accuracy amongst the other spectral bands combinations. The user's accuracy was not satisfactory for 50% of the categories, except the categories of *Pinus halepensis* (90.48%), maquis + rocks (85.00%), broadleaf's (93.33%), range (80.00%), urban areas (94.44%) and water (100.00%).

The spectral bands combination 4-6 (Table 3) gave the second lowest accuracy assessment. Misclassification errors appeared between the categories *Pinus Halepensis* and maquis, olive trees and agriculture, sand, and urban areas. The categories of the maquis, broadleaf's and sand were classified with the lowest accuracies of the various spectral bands combinations. The user's accuracy was satisfactory only for 42% of the categories (*Pinus nigra*, broadleaf's, range, urban areas, and water).

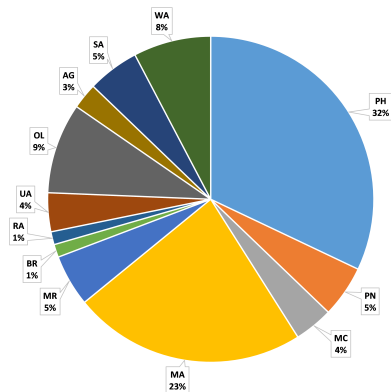
The spectral bands combination 3-4-5 (Table 4) gave overall accuracy (88.52%) while the classification errors appeared between the categories of sand and urban areas, olive trees and agriculture. The category of broadleaf gave the highest producers accuracy (100.00%) as the same percentage appeared with spectral bands combination 4-5-6 and 3-4-5-6-7. The user's accuracy was satisfactory for 42.00% pf the categories but it is noticeable that the categories of conifers gave user's accuracy between 93.48% (*Pinus halepensis*) and 97.96% (mixed conifers), which is satisfactory for forest purposes [17].

The spectral bands combinations 4-5-6 (Table 5) gave an overall accuracy of 96.29%, a little lower than the spectral bands combinations 3-4-5-6-7 (98.15%). The categories of mixed conifers, maquis, maquis + rocks, broadleaf, urban areas, and sand gave the highest procedure's accuracy among the various spectral bands combinations. Most (83.33%) of the categories gave user's accuracy more than 89% which is satisfactory [6, 19].

The spectral bands combinations 3-4-5-6 (Table 6) gave almost the same overall accuracy as spectral bands combination 3-7 (71.85 and 71.11 % respectively). Classification errors appeared between the categories of maquis and maquis + rocks, urban areas, and agriculture. The category urban areas gave the lowest producer's accuracy amongst the various spectral bands combinations.

Table 1: Matrix statistical separability for 3-5 spectral bands combination

Category	PH	PN	MC	MA	M+R	BR	RA	UA	OL	AG	SA	WA
PH	0.00	98.8	99.2	67.6	88.5	95.7	92.5	93.9	80.8	78.6	80.8	99.9
PN	98.8	0.00	75.3	97.5	98.6	99.7	99.7	100	99.4	98.0	99.9	99.9
MC	99.2	75.3	0.00	97.3	98.6	98.6	99.3	99.9	99.2	98.7	99.9	100.0
MA	67.6	97.5	97.3	0.00	0.00	94.2	89.4	95.4	67.6	67.4	97.8	100.0
M+R	88.5	98.6	98.6	80.7	96.3	96.3	74.3	83.4	75.7	76.9	95.6	100.0
BR	95.7	99.7	98.6	94.2	74.3	0.00	95.7	98.8	91.9	96.4	99.4	100.0
RA	92.5	99.7	99.3	89.4	83.4	95.7	0.00	85.3	68.8	90.2	96.6	100.0
UA	93.9	100.0	99.9	95.4	83.4	98.8	85.3	0.00	86.4	93.9	88.0	100.0
OL	80.8	99.4	98.6	77.3	75.7	91.9	68.8	86.4	0.00	82.4	96.4	100.0
AG	78.6	98.0	98.7	67.4	76.9	96.4	90.2	93.9	82.4	0.00	98.0	100.0
SA	97.0	99.9	99.0	97.8	95.6	99.4	96.6	88.0	96.4	98.0	0.00	100.0
WA	99.0	100.0	100.0	100.0	100.0	100.0	100.0	100.0	100.0	100.0	100.0	0.00
Sum of deviation	0.20	135.5	107.5	142.2	31.5	75.0	108.3	33.4	34.5	131.3	119.5	33.2



Where: PH: *Pinus halepensis*, PN: *Pinus nigra*, MC: mixed conifers, MA: maquis, MR: maquis + rocks, BR: broadleaf, RA: range, UA: urban area, OL: olive trees, AG: agriculture, SA: sand and WA: water

Figure 4: The contribution of the training fields in the classification

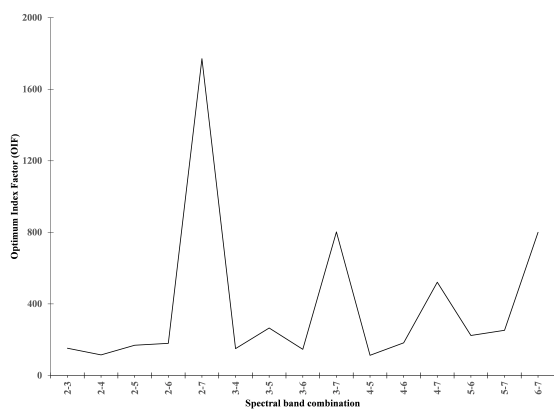


Figure 5: Two spectral bands combination

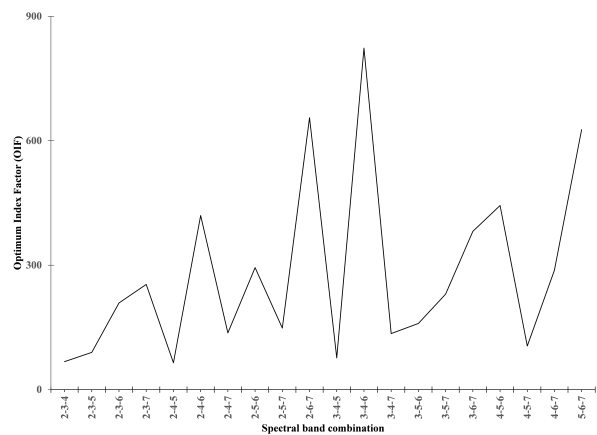


Figure 6: Three spectral bands combination

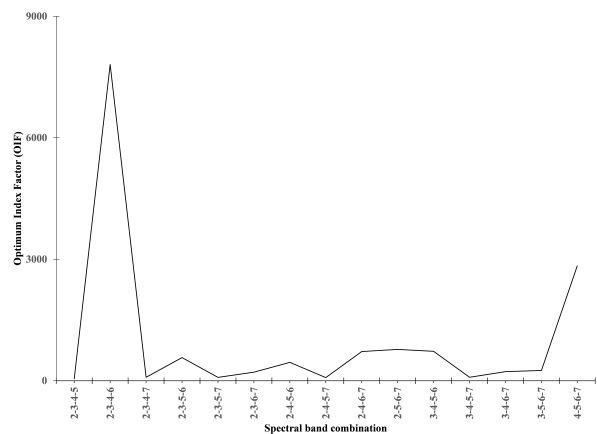


Figure 7: Four spectral bands combination

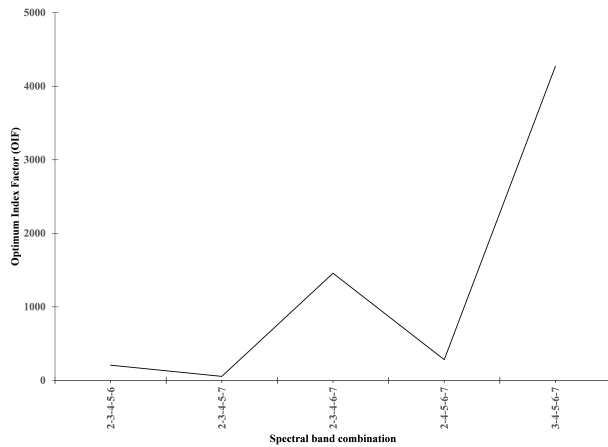


Figure 8: Five spectral bands combination

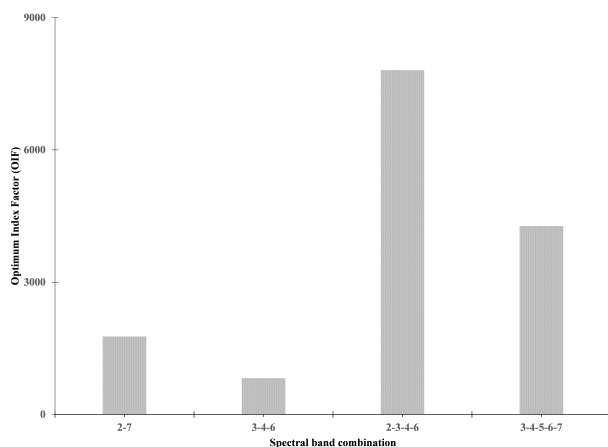


Figure 9: Best spectral bands combination, based on OIF

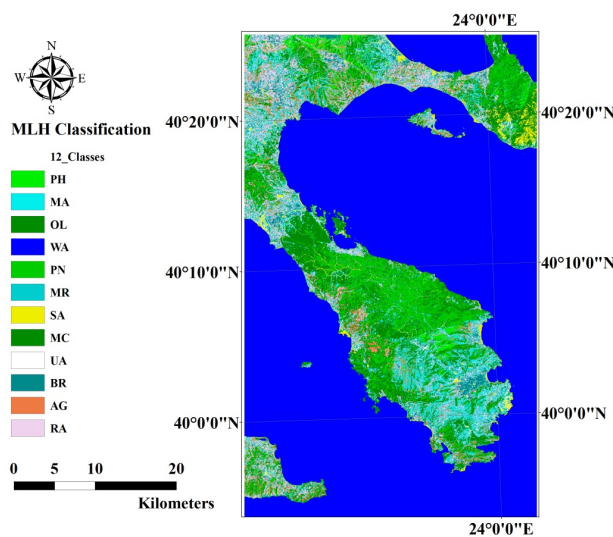


Figure 10: Maximum likelihood classification

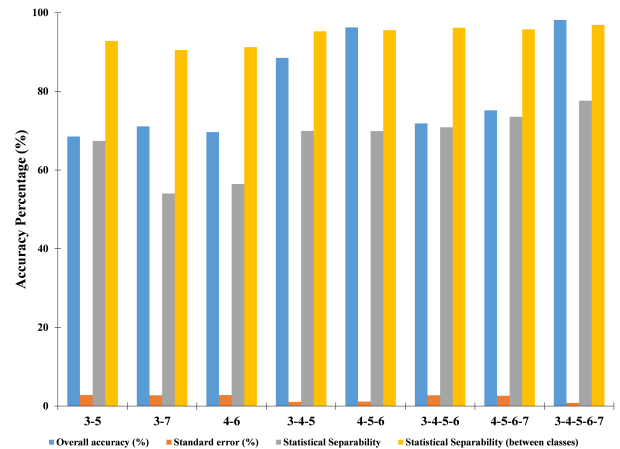


Figure 11: Overall accuracy assessment of various spectral bands combinations

The spectral bands combination 4-5-6-7 (Table 7) gave higher accuracy than the spectral bands combination 3-4-5-6 (75.18 and 71.85% respectively). Classification errors appeared between the categories of maquis and maquis + rocks, agriculture and olive trees.

The spectral bands combination 3-4-5-6-7 (Table 8) gave the highest overall accuracy (98.15%). The categories of *Pinus halepensis*, *Pinus nigra*, mixed conifers, maquis, broadleaf's, range, olive trees, agriculture, and sand gave the highest producer's accuracy amongst the various spectral bands combinations.

Results from the analysis indicated that all the three spectral regions are suitable for forest cover classification and mapping [13, 34]. The combination of the visible spectral bands with the near and middle infrared bands give more accurate mapping results [8, 24].

The visible range of the spectrum seemed separating forests from other categories, but differentiating results broadleaf and coniferous forests [1, 9]. The near and middle infrared give quite satisfactory results in separating the two forest categories from each other (*Pinus halepensis* and *Pinus nigra*), with some failures between the broadleaf's stands and the range [16, 18] (Figure 12).

4 Conclusions

Some authors claim to achieve better results with supervised than an unsupervised classification [7, 50]. It is easier to delineate well-defined classes by appropriately supervising techniques, but this requires a certain familiarity with the region. For areas, as large and complex as this study area, an unsupervised method must be used

Table 2: Matrix statistical separability for 3-7 spectral bands combination

Category	PH	PN	MC	MA	M+R	BR	RA	UA	OL	AG	SA	WA
PH	0.00	96.9	92.2	54.0	70.2	71.1	76.9	93.2	67.7	91.2	97.4	98.1
PN	96.9	0.00	77.5	96.2	98.4	99.3	99.8	100.0	99.6	95.6	99.9	100.0
MC	92.2	77.5	0.00	89.6	95.8	96.2	99.1	100.0	98.4	93.1	99.8	98.9
MA	54.0	96.2	96.2	0.00	71.8	69.5	82.4	95.4	73.2	92.5	98.0	98.9
M+R	70.2	98.4	98.4	71.8	0.00	84.8	67.0	81.1	63.8	97.3	94.0	99.8
BR	71.1	99.3	96.2	69.5	84.8	0.00	90.7	98.4	83.8	93.5	98.8	99.2
RA	76.9	99.8	99.1	82.4	81.1	90.7	0.00	81.1	61.3	99.1	95.4	100.0
UA	93.2	100.0	100.0	95.4	67.0	98.4	81.1	0.00	86.3	98.3	85.7	100.0
OL	67.7	99.6	98.4	73.2	81.1	83.8	61.3	86.3	0.00	96.4	96.2	99.9
AG	91.2	95.6	93.1	92.5	63.8	93.5	99.1	98.3	96.4	0.00	98.5	97.2
SA	97.4	99.9	99.8	98.0	94.0	98.9	95.4	85.7	96.2	98.5	0.00	100.0
WA	98.1	100.0	98.9	98.8	99.8	99.2	100.0	100.0	99.9	97.2	100.0	0.00
Sum of deviation	191.9	37.0	60.4	178.9	176.5	114.3	147.3	80.6	173.7	47.4	36.5	9.90

Table 3: Matrix statistical separability for 4-6 spectral bands combination

Category	PH	PN	MC	MA	M+R	BR	RA	UA	OL	AG	SA	WA
PH	0.00	95.5	89.8	56.5	70.0	100.0	86.6	93.1	77.4	92.4	95.7	99.7
PN	96.0	0.00	77.2	95.5	97.7	72.5	99.9	100.0	99.5	96.4	99.8	100.0
MC	92.4	77.2	0.00	89.8	95.2	82.3	99.5	100.0	98.5	96.8	99.6	100.0
MA	56.5	95.5	89.8	0.00	70.6	83.1	88.2	95.9	77.4	94.5	99.6	99.8
M+R	70.0	97.7	99.5	70.6	0.00	97.9	68.4	83.9	67.3	97.7	96.6	100.0
BR	82.3	98.0	93.5	72.5	80.8	0.00	92.4	98.5	83.1	98.9	90.3	100.0
RA	86.6	99.9	99.5	88.2	68.4	92.4	0.00	78.0	67.5	99.4	97.9	100.0
UA	93.1	100.0	100.0	95.9	83.9	98.0	78.0	0.00	87.2	97.7	88.7	100.0
OL	77.4	99.5	98.5	77.4	67.3	93.5	67.5	87.2	0.00	97.3	93.0	100.0
AG	92.4	96.4	96.8	94.5	97.7	80.8	99.4	97.7	97.3	0.00	98.8	100.0
SA	95.7	99.8	99.6	96.6	90.3	98.9	88.7	81.8	93.0	98.9	0.00	100.0
WA	99.7	100.0	100.0	99.8	100.0	0.0	100.0	100.0	100.0	100.0	100.0	0.00
Sum of deviation	158	40.0	57.3	162.6	178.1	102.0	131.4	83.9	152.0	29.9	57.0	0.60

Table 4: Matrix statistical separability for 3-4-5 spectral bands combination

Category	PH	PN	MC	MA	M+R	BR	RA	UA	OL	AG	SA	WA
PH	0.00	99.0	99.4	69.9	90.4	97.7	96.1	95.9	85.4	95.7	97.5	100.0
PN	99.0	0.00	78.7	98.0	99.3	99.8	99.9	100.0	99.7	98.2	100.0	100.0
MC	99.4	78.7	0.00	97.5	98.9	99.0	99.7	100.0	99.2	99.5	100.0	100.0
MA	69.9	98.0	97.5	0.00	81.9	95.8	92.8	96.6	80.3	95.5	98.1	100.0
M+R	90.4	99.3	98.9	81.9	0.00	96.8	80.7	86.1	77.9	98.0	96.3	100.0
BR	97.7	99.8	99.0	95.8	96.7	0.00	96.1	99.2	93.3	100.0	99.5	100.0
RA	96.1	99.9	99.7	92.8	80.7	96.1	0.00	89.5	71.5	99.8	97.4	100.0
UA	95.9	100.0	100.0	96.6	86.1	99.2	89.5	0.00	89.3	98.0	89.2	100.0
OL	85.4	99.7	99.2	80.3	77.9	93.3	71.5	89.3	0.00	97.9	96.7	100.0
AG	95.7	98.2	99.5	95.5	98.0	100.0	99.8	98.0	97.9	0.00	99.4	100.0
SA	97.5	100.0	100.0	98.1	96.3	99.5	97.4	89.2	96.7	99.4	0.00	100.0
WA	100.0	100.0	100.0	100.0	100.0	100.0	100.0	100.0	100.0	100.0	100.0	0.00
Sum of deviation	73.1	27.5	28.3	93.5	93.8	22.9	76.5	56.2	108	18.1	25.9	0.00

Table 5: Matrix statistical separability for 4-5-6 spectral bands combination

Category	PH	PN	MC	MA	M+R	BR	RA	UA	OL	AG	SA	WA
PH	0.00	98.8	99.1	69.9	88.6	96.9	93.2	95.4	84.8	95.8	95.8	100.0
PN	98.8	0.00	80.5	98.0	99.3	99.6	100.0	100.0	99.7	98.0	100.0	100.0
MC	99.1	80.5	0.00	97.2	98.9	98.9	99.8	100.0	99.1	99.3	99.9	100.0
MA	69.9	98.0	97.2	0.00	79.8	95.2	91.2	96.8	80.7	95.8	97.0	100.0
M+R	88.6	99.3	98.9	79.8	0.00	96.2	70.9	85.7	76.8	97.9	94.1	100.0
BR	96.6	99.6	98.9	95.2	96.2	0.00	96.6	99.2	92.4	99.9	99.1	100.0
RA	93.2	100.0	99.8	91.2	70.9	96.6	0.00	79.8	71.8	99.5	92.4	100.0
UA	95.4	100.0	100.0	96.8	85.7	99.2	79.8	0.00	88.7	98.2	86.4	100.0
OL	84.8	99.7	99.1	80.7	76.8	92.4	71.8	88.7	0.00	98.0	94.3	100.0
AG	95.8	98.0	99.8	95.8	97.9	99.9	99.5	98.2	98.0	0.00	99.3	100.0
SA	95.8	100.0	99.9	97.0	94.1	99.1	92.4	86.4	94.3	99.3	0.00	100.0
WA	100.0	100.0	100.0	100.0	100.0	100.0	100.0	100.0	100.0	100.0	100.0	0.00
Sum of deviation	81.8	26.1	27.3	98.2	111.6	25.9	104.9	69.9	113.7	18.3	41.7	0.00

Table 6: Matrix statistical separability for 3-4-5-6 spectral bands combination

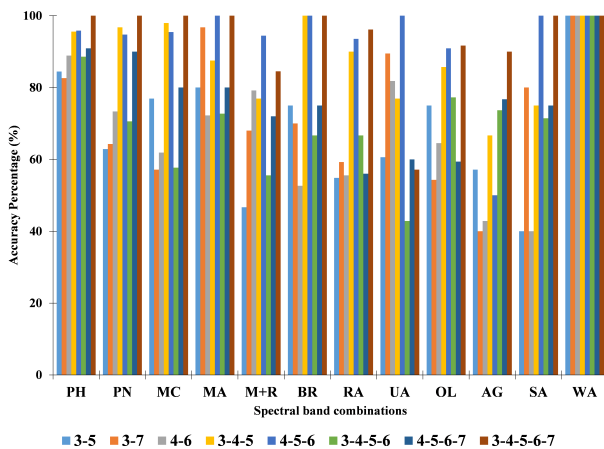
Category	PH	PN	MC	MA	M+R	BR	RA	UA	OL	AG	SA	WA
PH	0.00	99.3	99.2	70.9	90.8	97.9	97.6	96.2	86.0	96.0	98.6	100.0
PN	99.3	0.00	81.2	98.4	99.4	99.7	100.0	100.0	99.8	98.6	100.0	100.0
MC	99.4	81.2	0.00	97.7	99.0	99.0	99.8	100.0	99.2	99.5	100.0	100.0
MA	70.9	98.4	97.7	0.00	82.7	96.2	96.5	97.1	81.8	96.0	98.6	100.0
M+R	90.8	99.4	99.0	82.7	0.00	96.8	91.1	87.6	78.7	98.2	96.8	100.0
BR	97.9	99.8	99.0	96.2	96.8	0.00	97.2	99.4	93.5	100.0	99.7	100.0
RA	97.6	100.0	99.8	96.5	91.1	97.2	0.00	93.1	85.6	99.9	98.7	100.0
UA	96.2	100.0	100.0	97.1	87.6	99.4	93.1	0.00	91.0	98.3	92.6	100.0
OL	86.0	99.8	99.2	81.8	78.7	93.5	85.6	91.0	0.00	98.1	97.9	100.0
AG	96.0	98.6	99.5	96.0	98.2	100.0	99.9	98.3	98.1	0.00	99.6	100.0
SA	98.6	100.0	100.0	98.6	96.8	99.7	98.7	92.6	97.7	99.6	0.00	100.0
WA	100.0	100.0	100.0	100.0	100.0	100.0	100.0	100.0	100.0	100.0	100.0	0.00
Sum of deviation	67.4	23.5	25.1	84.2	79.0	20.5	40.5	44.7	88.5	15.8	17.6	0.00

Table 7: Matrix statistical separability for 4-5-6-7 spectral bands combination

Category	PH	PN	MC	MA	M+R	BR	RA	UA	OL	AG	SA	WA
PH	0.00	99.4	99.5	77.0	90.6	97.8	95.7	96.5	89.0	97.0	97.3	100.0
PN	99.4	0.00	83.9	98.5	99.5	99.7	100.0	100.0	99.8	98.2	100.0	100.0
MC	99.5	83.9	0.00	97.5	98.9	99.1	99.9	100.0	99.2	99.3	100.0	100.0
MA	77.0	98.5	97.5	0.00	80.2	95.8	93.7	97.9	83.1	96.1	97.9	100.0
M+R	90.6	99.5	98.9	80.2	0.00	96.6	79.9	90.1	79.6	98.1	95.6	100.0
BR	97.8	99.7	99.1	95.8	96.6	0.00	97.2	99.6	93.4	100.0	99.3	100.0
RA	95.7	100.0	99.9	93.7	79.9	97.2	0.00	89.9	73.5	99.6	94.4	100.0
UA	96.5	100.0	100.0	9.8	90.1	99.6	89.9	0.00	93.2	99.4	89.0	100.0
OL	89.0	99.8	99.2	83.1	79.6	93.4	73.5	93.2	0.00	98.3	95.5	100.0
AG	97.0	98.2	99.3	96.1	98.1	100.0	99.6	99.4	98.3	0.00	99.6	100.0
SA	97.3	100.0	100.0	97.9	95.6	99.3	94.4	89.0	95.5	99.6	0.00	100.0
WA	100.0	100.0	100.0	100.0	100.0	100.0	100.0	100.0	100.0	100.0	100.0	0.00
Sum of deviation	60.3	21.1	28.8	82.3	90.8	21.6	76.2	44.4	95.3	14.3	31.5	0.00

Table 8: Matrix statistical separability for 3-4-5-6-7 spectral bands combination

Category	PH	PN	MC	MA	M+R	BR	RA	UA	OL	AG	SA	WA
PH	0.00	99.6	99.7	77.6	92.5	98.4	98.1	97.1	89.7	97.2	98.8	100.0
PN	99.6	0.00	84.4	98.8	99.5	99.9	100.0	100.0	99.8	98.8	100.0	100.0
MC	99.7	84.4	0.00	97.9	99.0	99.2	99.9	100.0	99.3	99.6	100.0	100.0
MA	77.6	99.8	97.7	0.00	83.2	96.6	97.0	98.1	83.8	96.2	99.0	100.0
M+R	92.5	99.5	99.0	83.2	0.00	97.1	92.2	91.5	81.1	98.5	97.6	100.0
BR	98.4	99.9	99.2	96.6	97.1	0.00	97.6	99.7	94.4	100.0	99.8	100.0
RA	98.1	100.0	99.9	97.0	92.2	97.6	0.00	96.5	85.9	99.9	99.3	100.0
UA	97.1	100.0	100.0	98.1	91.5	99.7	96.5	0.00	94.9	99.5	93.6	100.0
OL	89.7	99.8	99.3	83.8	81.1	94.4	85.9	94.9	0.00	98.4	98.5	100.0
AG	97.2	98.8	99.6	96.2	98.5	100.0	99.9	99.5	98.4	0.00	99.7	100.0
SA	98.8	100.0	100.0	99.0	97.6	99.8	99.3	93.6	98.5	99.7	0.00	100.0
WA	100.0	100.0	100.0	100.0	100.0	100.0	100.0	100.0	100.0	100.0	100.0	0.00
Sum of deviation	58.6	19.7	26.3	97.9	85.2	19.5	75.1	42.5	91.6	13.1	27.4	0.00



Where: PH: *Pinus halepensis*, PN: *Pinus nigra*, MC: mixed conifers, MA: maquis, MR: maquis + rocks, BR: broadleaf, RA: range, UA: urban area, OL: olive trees, AG: agriculture, SA: sand and WA: water

Figure 12: Classification accuracy assessment of different categories of various spectral bands combinations

initially to obtain an indication of the spectral variability of the various categories. Once the unsupervised classification gives a general knowledge of the study area, then the supervised classification will yield greater accuracy in separating forest types, which most of the time have reflectances values close to each other. By utilizing the visible, near and mid-infrared parts of the electromagnetic spectrum gave an overall accuracy more than 98.10% can be achieved. High classification accuracies ranging from 82.61% to 98.15% for the *Pinus halepensis* category resulted from the analysis of the various spectral bands combination. For the category of *Pinus nigra*, the classification overall accuracy ranged between 62.86% and 96.77% while the mixed conifers between 57.14% and 95.45%. The category

of maquis can be classified and mapped with accuracies ranging from 72.22% to 100%; the category of maquis + rocks lead to misclassification results, due to the presence of different amount of rocks which affected the spectral behavior of this category. The broadleaf's classified, with overall accuracy ranging between 52.63% and 100%. The range category can be classified with accuracies ranging from 54.84% to 96.15%; the lower limit was due to classification errors between this category and maquis category, as in Sithonia there are not improved pasture, but only degraded forested lands where maquis predominate. The olive trees and agriculture categories lead several times to classification errors, due to the similar spectral response. The agricultural lands showed the lowest overall accuracy (40% in spectral bands combination 3-7). The category sand showed the lowest accuracy (40%) in spectral bands combination 3-5 and 4-6. This category was confused with the category of urban areas due to the coarse resolution of the image (mixed pixel).. Water, on the contrary, was classified with the highest accuracy (100%). Finally, it seems that, spectral bands 3-4-5-6-7 are the most suitable for forest inventories. It should be noticed that more detailed inventory during the development of the training sites should have been done because the classification proved the presence of broadleaf's in ravines, where no training data were collected.

Acknowledgement: This article was funded by the Deanship of Scientific Research (DSR) at King Abdulaziz University, Jeddah. The authors, therefore, acknowledged with thanks DSR for technical and financial support.

The author declares no conflict of interest regarding the publication of this manuscript.

References

- [1] Nelson, R.F., R. Latty, and G. Mott, Classifying northern forests using Thematic Mapper simulator data. 1984.
- [2] Yuan, F., et al., Multi-level land cover mapping of the Twin Cities (Minnesota) metropolitan area with multi-seasonal Landsat TM/ETM+ data. *Geocarto International*, 2005. 20(2): p. 5-13.
- [3] Tou, J. and R. Gonzales, *Pattern Recognition Principles*. Addison-Wesley. Reading, MA, 1974. 377.
- [4] Spanner, M.A., J.A. Brass, and D.L. Peterson, Feature selection and information content of thematic mapper simulator data for a forested environment. 1983.
- [5] Clinton, N., et al., Accuracy assessment measures for object-based image segmentation goodness. *Photogrammetric Engineering and remote sensing*, 2010. 76(3): p. 289-299.
- [6] Rogan, J., et al., Land-cover change monitoring with classification trees using Landsat TM and ancillary data. *Photogrammetric Engineering & Remote Sensing*, 2003. 69(7): p. 793-804.
- [7] Elhag, M., A. Psilovikos, and M. Sakellariou, Detection of land cover changes for water resources management using remote sensing data over the Nile Delta Region. *Environment, Development and Sustainability*, 2013. 15(5): p. 1189-1204.
- [8] Friedl, M.A., et al., MODIS Collection 5 global land cover: Algorithm refinements and characterization of new datasets. *Remote sensing of Environment*, 2010. 114(1): p. 168-182.
- [9] Ghimire, B., J. Rogan, and J. Miller, Contextual land-cover classification: incorporating spatial dependence in land-cover classification models using random forests and the Getis statistic. *Remote Sensing Letters*, 2010. 1(1): p. 45-54.
- [10] Congalton, R.G. and K. Green, *Assessing the accuracy of remotely sensed data: principles and practices*. 2008: CRC press.
- [11] Townshend, J.R., et al., Global characterization and monitoring of forest cover using Landsat data: opportunities and challenges. *International Journal of Digital Earth*, 2012. 5(5): p. 373-397.
- [12] Richards, J.A. and J. Richards, *Remote sensing digital image analysis*. Vol. 3. 1999: Springer.
- [13] Gislason, P.O., J.A. Benediktsson, and J.R. Sveinsson, Random forests for land cover classification. *Pattern Recognition Letters*, 2006. 27(4): p. 294-300.
- [14] Betts, R.A., et al., Biogeophysical effects of land use on climate: Model simulations of radiative forcing and large-scale temperature change. *Agricultural and forest meteorology*, 2007. 142(2): p. 216-233.
- [15] Chapman, D.S., et al., Random Forest characterization of upland vegetation and management burning from aerial imagery. *Journal of Biogeography*, 2010. 37(1): p. 37-46.
- [16] Hansen, M.C., et al., High-resolution global maps of 21st-century forest cover change. *science*, 2013. 342(6160): p. 850-853.
- [17] Gong, P., et al., Finer resolution observation and monitoring of global land cover: First mapping results with Landsat TM and ETM+ data. *International Journal of Remote Sensing*, 2013. 34(7): p. 2607-2654.
- [18] Lunetta, R.S. and M.E. Balogh, Application of multi-temporal Landsat 5 TM imagery for wetland identification. *Photogrammetric Engineering and Remote Sensing*, 1999. 65(11): p. 1303-1310.
- [19] Li, C., et al., Comparison of classification algorithms and training sample sizes in urban land classification with Landsat thematic mapper imagery. *Remote Sensing*, 2014. 6(2): p. 964-983.
- [20] Davis, S.M., et al., *Remote sensing: the quantitative approach*. New York, McGraw-Hill International Book Co., 1978. 405 p., 1978. 1.
- [21] Manolakis, D. and G. Shaw, Detection algorithms for hyperspectral imaging applications. *IEEE signal processing magazine*, 2002. 19(1): p. 29-43.
- [22] Mallinis, G., et al., Forest parameters estimation in a European Mediterranean landscape using remotely sensed data. *Forest Science*, 2004. 50(4): p. 450-460.
- [23] Gausman, H., et al., Reflectance discrimination of cotton and corn at four growth stages. *Agronomy Journal*, 1973. 65(2): p. 194-198.
- [24] Lathrop, R., T.M. Lillesand, and B.S. Yandell, An evaluation of Thematic Mapper data for forest cover mapping in northern Wisconsin. *Proc. 11th Pecora Sym.*, Sioux Falls, SD, 1987: p. 386-393.
- [25] Elhag, M., Evaluation of different soil salinity mapping using remote sensing techniques in arid ecosystems, Saudi Arabia. *Journal of Sensors*, 2016. 2016.
- [26] Murtha, P. and E. Watson. Mapping of forest clear-cutting, south Vancouver Island, from Landsat imagery. in *Canadian Symposium on Remote Sensing*, 3 rd, Edmonton, Alberta, Canada. 1976.
- [27] Coggeshall, M.E. and R.M. Hoffer, Basic forest cover mapping using digitized remote sensor data and automated data processing techniques. 1973.
- [28] Duda, R.O., P.E. Hart, and D.G. Stork, *Pattern classification*. Vol. 2. 1973: Wiley New York.
- [29] Briem, G.J., J.A. Benediktsson, and J.R. Sveinsson, Multiple classifiers applied to multisource remote sensing data. *IEEE transactions on geoscience and remote sensing*, 2002. 40(10): p. 2291-2299.
- [30] Lippitt, C.D., et al., Mapping Selective Logging in Mixed Deciduous Forest. *Photogrammetric Engineering & Remote Sensing*, 2008. 74(10): p. 1201-1211.
- [31] Franklin, S. and M. Wulder, Remote sensing methods in medium spatial resolution satellite data land cover classification of large areas. *Progress in Physical Geography*, 2002. 26(2): p. 173-205.
- [32] Bonan, G.B., Forests and climate change: forcings, feedbacks, and the climate benefits of forests. *science*, 2008. 320(5882): p. 1444-1449.
- [33] Steele, B.M., Combining multiple classifiers: An application using spatial and remotely sensed information for land cover type mapping. *Remote sensing of environment*, 2000. 74(3): p. 545-556.
- [34] Rogan, J., et al., Mapping land-cover modifications over large areas: A comparison of machine learning algorithms. *Remote Sensing of Environment*, 2008. 112(5): p. 2272-2283.
- [35] Huang, H., et al., Reduction of atmospheric and topographic effect on Landsat TM data for forest classification. *International Journal of Remote Sensing*, 2008. 29(19): p. 5623-5642.
- [36] Coppin, P.R. and M.E. Bauer, Digital change detection in forest ecosystems with remote sensing imagery. *Remote sensing reviews*, 1996. 13(3-4): p. 207-234.
- [37] Hopkins, P.F., A.L. Maclean, and T.M. Lillesand, Assessment of Thematic Mapper imagery for forestry applications under Lake

- States conditions. *Photogrammetric Engineering and Remote Sensing*, 1988. 54(1): p. 61-68.
- [38] Bonazountas, M., et al., A decision support system for managing forest fire casualties. *Journal of Environmental Management*, 2007. 84(4): p. 412-418.
- [39] Chavez Jr, P.S., G.L. Berlin, and L.B. Sowers, Statistical Method for Selecting Landsat MSS. *Journal of applied photographic engineering*, 1982. 8(1): p. 23-30.
- [40] DeFries, R. and J.C.-W. Chan, Multiple criteria for evaluating machine learning algorithms for land cover classification from satellite data. *Remote Sensing of Environment*, 2000. 74(3): p. 503-515.
- [41] Cutler, D.R., et al., Random forests for classification in ecology. *Ecology*, 2007. 88(11): p. 2783-2792.
- [42] Elhag, M. and J.A. Bahrawi, Conservational use of remote sensing techniques for a novel rainwater harvesting in arid environment. *Environmental earth sciences*, 2014. 72(12): p. 4995-5005.
- [43] Sesnie, S.E., et al., Integrating Landsat TM and SRTM-DEM derived variables with decision trees for habitat classification and change detection in complex neotropical environments. *Remote Sensing of Environment*, 2008. 112(5): p. 2145-2159.
- [44] Foody, G.M., Sample size determination for image classification accuracy assessment and comparison. *International Journal of Remote Sensing*, 2009. 30(20): p. 5273-5291.
- [45] Petropoulos, G., et al., A global Bayesian sensitivity analysis of the 1d SimSphere soil-vegetation-atmospheric transfer (SVAT) model using Gaussian model emulation. *Ecological Modelling*, 2009. 220(19): p. 2427-2440.
- [46] Elhag, M., Inconsistencies of SEBS Model Output Based on the Model Inputs: Global Sensitivity Contemplations. *Journal of the Indian Society of Remote Sensing*, 2016. 44(3): p. 435-442.
- [47] Psilovikos, A. and M. Elhag, Forecasting of remotely sensed daily evapotranspiration data over Nile Delta region, Egypt. *Water Resources Management*, 2013. 27(12): p. 4115-4130.
- [48] Elhag, M. and J.A. Bahrawi, Soil salinity mapping and hydrological drought indices assessment in arid environments based on remote sensing techniques. *Geoscientific Instrumentation, Methods and Data Systems*, 2017. 6(1): p. 149.
- [49] Congalton, R.G., A review of assessing the accuracy of classifications of remotely sensed data. *Remote sensing of environment*, 1991. 37(1): p. 35-46.
- [50] Elhag, M. and J.A. Bahrawi, Realization of daily evapotranspiration in arid ecosystems based on remote sensing techniques. *Geoscientific Instrumentation, Methods and Data Systems*, 2017. 6(1): p. 141.